Atom-by-atom fabrication with electron beams

NATREVMATS-19-739V1

Atom-by-atom Fabrication with Electron Beams

Ondrej Dyck,[1] Maxim Ziatdinov,[1,2] David Lingerfelt,[1] Raymond R. Unocic,[1] Bethany M. Hudak,[1] Andrew R. Lupini,[1] Stephen Jesse,[1] Sergei V. Kalinin[1]

[1] Center for Nanophase Materials Sciences, Oak Ridge National Laboratory, Oak Ridge, TN

[2] Computational Sciences and Engineering Division, Oak Ridge National Laboratory, Oak Ridge, TN

Abstract: Assembling matter atom-by-atom into functional devices is the ultimate goal of nanotechnology. The possibility of achieving this goal is intrinsically dependent on the ability to visualize matter at the atomic level, induce and control atomic-scale motion, facilitate and direct chemical reactions, and coordinate and guide fabrication processes towards desired structures atom-by-atom. In this review, we summarize recent progress in chemical transformations, material alterations and atomic dynamics studies enabled by the converged, atomic-sized electron beam of an aberration-corrected scanning transmission electron microscope. We discuss how such "top down" observations have led to the concept of controllable, beam-induced processes and then of "bottom up" atom-by-atom assembly via electron beam control. The progress in this field, from electron-beam-induced material transformations to atomically precise doping and multi-atom assembly, is reviewed, as are the associated engineering, theoretical, and big-data challenges.

Introduction: Assembling matter atom-by-atom is the ultimate goal of nanotechnology, as set forth in Feynman's visionary speech in 1959.[1] The first ever experimental demonstration of atom-by-atom assembly via the metallic tip of a scanning tunneling microscope (STM) by Eigler at IBM in 1990[2] made atomic manipulation a reality and arguably launched the modern era of nanotechnology. During the last several years, this field has achieved paramount importance due to technological drivers, such as quantum computing and sensing. However, the transition from proof-of-concept experiments to fabrication of practical qubit devices, such as those produced by Simmons at the University of New South Wales,[3] proved to be no small task. STM and its intrinsically surface nature necessitated the combination of STM with advanced surface science and mesoscale fabrication methods to achieve this level of control. Recent progress toward the fabrication of thermally stable rudimentary circuit elements in a hydrogen-terminated silicon surface has leveraged deterministic positioning of dangling bonds aided by machine learning approaches to produce a "binary wire" and an OR gate.[4] Atomic force microscopy (AFM) has also achieved similar atomic level control by being able to pick up and replace atoms on surfaces.[5-8] Some investigations have also alternated between employing AFM and STM techniques.[9] Alternatively, the "molecular machines" approach toward atomistic fabrication harnesses the power of modeling and synthetic chemistry to build individual functional blocks,[10,11] yet strategies for assembly of these blocks remain uncertain. The progress in this field is perhaps best exemplified by the 2016 Nobel prize in Chemistry "for the design and synthesis of molecular machines."[12]

Another paradigm of nanotechnology has recently emerged,[13] which uses the focused electron beam of a scanning transmission electron microscope (STEM) to control and direct matter at the single atom level. STEMs are conventionally used as a materials characterization tool for

imaging, diffraction, and spectroscopy, where beam-induced modifications of the material are perceived as creating undesirable and uncontrolled damage.[14,15] However, it was recently demonstrated that multimodal STEM data can be analyzed with precision on the order of picometers, providing a comprehensive picture of local structure and chemical bonding,[16-18] and that beam effects on materials can be controlled and exploited to induce ordering of oxygen vacancies,[19] form single vacancies in two dimensional (2D) materials,[20] and stimulate beam-induced migration of single impurity atoms.[21] Based on STEM observations and by taking advantage of the synergy with SPM-based fabrication, such effects can be harnessed to directly control atomic configurations in a solid. Exquisite beam control and rapid feedback based on image analytics have been implemented to create single-digit nanometer structures that can be formed and imaged with atomic resolution, as first demonstrated in strontium titanate[22] and more recently in bulk Si: within the last year, this approach was used to demonstrate the controllable motion of dopant fronts in bulk Si[23] and the incorporation of single Si atoms in the lattice of graphene,[24-27] leading to the controllable formation of dimer, trimer and tetramer structures.[28]

Here, we survey recent demonstrations of electron-beam induced transformations on the level of individual atoms and atomic bonds. We illustrate that while never compiled in an integrated cause and effect table, the spectrum of electron beam induced atomic transformations is remarkably broad, opening a plethora of capabilities of controlled beam induced chemistry. Harnessing these in a systematic manner opens a pathway towards atom-by-atom fabrication in a STEM. We also highlight developments with beam control and feedback and machine-learning-based automated data analysis necessary to implement this vision. Finally, we provide our perspective on how these tools will fit together to enable such developments as atomic-scale robotics and atomically precise manufacturing.

Enabling Developments: Several significant achievements have converged to form the fabric of our present understanding and technological expertise. Technical developments realized over the past two decades enable state-of-the-art STEMs to image and analyze single atoms, propelling scientific discovery to a new level.

Aberration Correction: One of the most notable advances in the field of STEMs has been the successful introduction and widespread adoption of aberration correction,[29] which ultimately allowed for the resolution to be increased from what was previously termed high-resolution or atomic resolution, e.g., ~2.2 Å, the theoretical Scherzer resolution limit calculated for a specific microscope,[30,31] to ~0.5 Å[32,33] with a corresponding increase in beam fluence. Historical reviews of the development of aberration correction are available in the literature[34-36] and will not be repeated here; however, it should be noted that the date of the first *proposal* for aberration correction (Scherzer 1947[30]) can be contrasted with the first successful *demonstration* of aberration correction in a transmission electron microscope (TEM) (Haider *et al.* 1998 [37]) that occurred in parallel with the first *implementation* of aberration correction in a STEM (Krivanek, *et al.* 1999[38]), which were followed by the commercial adoption of aberration-corrected TEM/STEMs in the early 2000s. Far from being unproductive for a half-century prior to the wide integration of aberration correctors, electron microscopy advancements continued (see for example Pennycook and Nellist Chapter 1.3 *The Crewe Innovations* [31]), including the development of transformative techniques such as Z-contrast STEM imaging (Z is the atomic number) and atomically resolved electron energy loss spectroscopy (EELS) and energy dispersive X-ray spectroscopy (EDS). The development of aberration correction necessitated the advancement of two significant enabling parallel technologies before becoming feasible and to some extent, routine: the modern computer and digital imaging capabilities. These two critical technologies now go hand-in-hand with many

recent developments in the field of microscopy dealing primarily with imaging and diffraction data. Once computers could be purchased (at a reasonable cost) and images could be acquired and processed digitally, it became possible to develop automated analytical routines to extract information *in real time*. These advances are precisely what aberration correction needed to be effectively implemented and adopted by the community: the automated measurement and optimization of lens parameters in a short amount of time.[38,39]

The Rise of 2D Materials: Developments in the realm of materials synthesis have also played a significant role in setting the stage for atom-by-atom manipulation in the STEM. The isolation and characterization of graphene by Geim and Novoselov[40-42] launched the field of 2D materials and ultimately won them the 2010 Nobel Prize in physics. While graphene is certainly the most famous 2D material, new 2D materials are being fabricated at a rapid rate, including hexagonal boron nitride,[43] transition metal dichalcogenides,[44] phosphorene,[45] arsenene,[46] antimonene,[46] bismuthene,[46] silicene,[47] germanene,[48] iron,[49] zinc oxide,[50] molybdenum,[51] and MXenes.[52] The attractiveness of 2D materials as seen from the perspective of atom-by-atom fabrication in the STEM is that during imaging and analysis, it is straightforward to ascertain the crystallographic position and elemental identification of each atom.[53] With extended three dimensional (3D) crystalline (or amorphous) structures the precise geometry and elemental specification can many times be difficult to elucidate.[54,55] Moreover, 2D materials enable the possibility of exposing the entire material to external gas phase precursors to stimulate chemical reactions and beam-induced processes including deposition at a specific location.[56,57] Thus, the use of 2D materials coupled with the decreased (sub-Å) probe size provided by aberration correction in STEM allows us not only to determine the exact position and elemental identity of every atom in the 2D material, but

also provides the ability to precisely position the electron probe onto single atoms in the structure and induce precise alterations.

In situ Manipulation: A third development that has positioned the STEM as an atomic fabrication platform is the widespread adoption of unique *in situ* sample holders, which have enabled a variety of environmental parameters to be included in STEM analyses, including heating, cooling, electrical and magnetic biasing, liquid and gas cells, and nano-manipulators. These systems allow one to control the local sample environment while simultaneously acquiring images and

Phenomenon	Material System	Result	Year	Reference
Doping	h-BN nanosheets, nanoribbons, and nanotubes	Substitutional C doping	2011	56
	Graphene	Single Si dopants positioned	2017	24
Sculpting	Ni/Cr alloy, Ni, Cr, Au, Ag, Al	*In situ* device fabrication	2007	58
	Single layer MoS_2, $MoSe_2$, WSe_2	Nanowire formation	2013, 2014	59,60
	Graphene	Single atom wide chains	2009	61,62
	Single layer h-BN	Single atom wide chains	2014	63
	Few-layer black P	Single atom wide chains	2017	64
	Au foil	4 atom wide nanowire	1997	65
	Few-layer graphene	Holes and nanoribbons	2008, 2011	66,67
Directed Single Atom Movement	Si in graphene	Si atom moved through lattice	2017, 2018	24,25,27
	Bi in Si	Bi dopants moved through lattice	2018	68
	Si on graphene edges	Si atoms attached to graphene edge	2018	69
	P in graphene	P atom moved through lattice	2018	70
Crystal Growth	Amorphous Si, Ge, GaP, and GaAs	Amorphous to crystal transformation	1995, 2018	23,71
	Apatite $Sr_2Nd_8(SiO_4)_6O_2$	Recrystalization	2007	72
	Si and Ge	Recrystalization of ion implantation damage	1999	73
	CdTe thin films	Hexagonal quantum dot crystals	2009	74
	a-GaAs foil	Polynucleation and epitaxial growth	1997	75
	a-GeSi film	Various crystal structures	2005	76
	Mg-Ni	Mg NiH and MgH crystal growth	2014	77
	a-$SrTiO_3$/x-$SrTiO_3$	Patterned $SrTiO_3$ crystalline nanostructures	2015	22

Deposition	Aqueous solution of H_2PdCl_4	Direct-write of Pd nanostructures	2016	78
	Aqueous solution of $SiCl_4$	Deposition of Si nanostructures	2012	79
	Aqueous solutions of chloroplatinic acid	Deposition of Pt nanostructures	2011	80
	Silica nanoparticle suspension	Clustering of silica nanoparticles	2014	81
	Precursor gas $W(CO)_6$	Deposition of W nanostructures	2004, 2011, 2012	57,82,83
	Hydrocarbon on graphene	a-C and graphitic lettering	2018	84

Table 1 A collection of e-beam induced material transformations observed in (S)TEM with references to the corresponding publications.

spectroscopic data from the sample and documenting relevant changes. When coupled with the modifications induced by the electron beam itself,[14] an incredible range of material phenomena have been observed. In the next section we aim to impress upon the reader a sense of the wide array of phenomena within reach of the STEM.

***In situ* Phenomena:** We have condensed many examples of *in situ,* beam-induced phenomena into Table 1. For the sake of brevity this is not exhaustive; however, we attempt to underscore the rich array of experiments that have been performed using electron beam irradiation in TEM and STEM. A more extensive table of beam-induced phenomena observed in TEM and STEM is available in the supplementary Table S1.

Recent Progress in STEM Fabrication: A wide variety of alterations can be made without a STEM. Growth and doping of 2D materials, for example, do not require using a STEM, especially a costly aberration-corrected STEM. However, using an atomic resolution STEM (or scanning probe microscopy instrument) gives a unique advantage: the ability to manipulate single atoms and produce alterations at the atomic scale in a highly controlled manner. One might argue that chemical vapor deposition processes, for example, act at the atomic scale in that growth occurs atom-by-atom. However, the control parameters, such as temperature or chemical environment, are applied on a macroscopic scale and it is the behavior of the macroscopic system as a whole

that enables tailored growth to occur. In a STEM, similar control parameters exist, with the addition of the atom-sized, focused electron beam, which causes the localized region of the sample under irradiation to experience a different environment than the unexposed regions of the sample. Thus, the STEM can be seen as producing the smallest possible reaction chamber in which a wide variety of transformations can be promoted and produced. It is also worth mentioning that electron beam exposure can not only induce transitions to lower energy states (such as crystallization), but can also induce transitions into higher energy states, for example, the metastable 1T-phase in MoS_2[85] or Stone-Wales (and other) defects in graphene.[86,87] In the rest of this section, we provide some noteworthy examples of experiments that have thrust aberration corrected STEM into the arena of atomic fabrication.

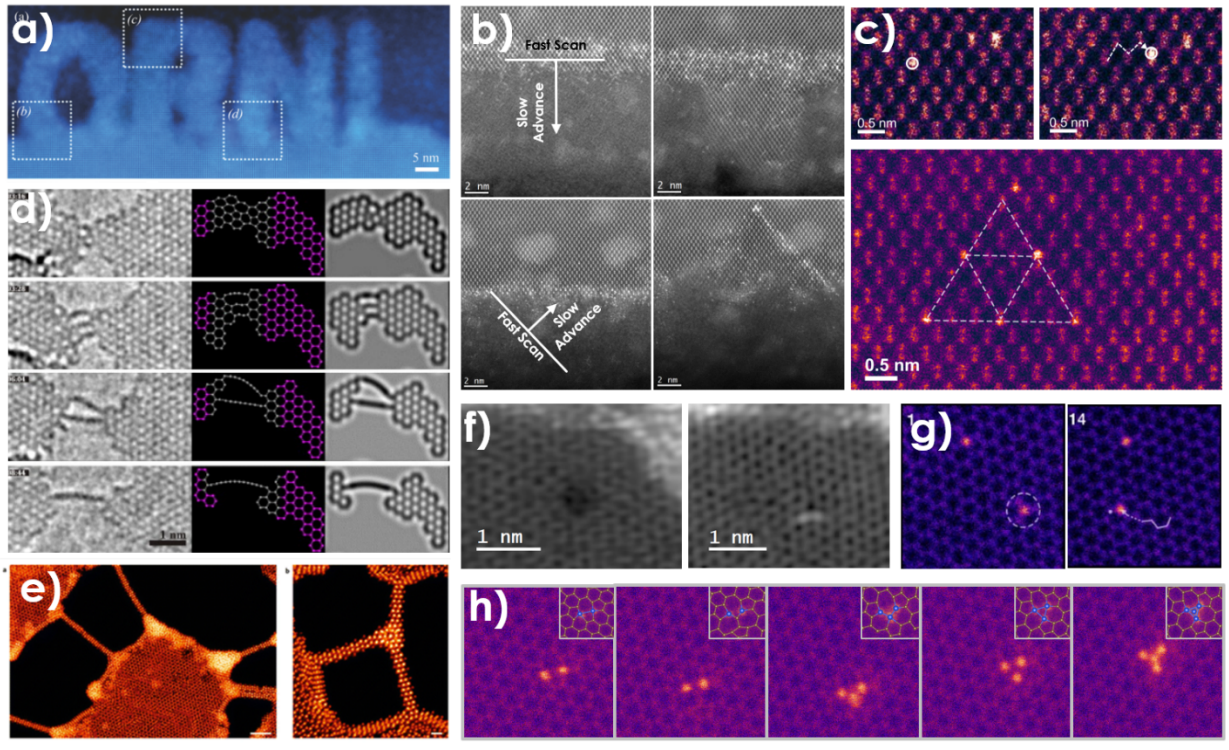

Figure 1 Collection of several key examples of atomic scale fabrication using electron beams. The result shown in a) illustrates the ability to crystalize amorphous strontium titanate in epitaxial registration with the strontium titanate substrate crystal (reprinted from Jesse *et al.*[22] 2015, *Small* with permission from John Wiley and Sons). Crystallization was performed layer-by-layer using a real-time analysis and feedback loop, which enabled automated control of the crystal/amorphous growth front. b) Jesse *et al.*,[23] extended the controlled crystal growth to include Si as well as observing electron beam-mediated movement of Bi dopants within

the Si crystal (Reproduced with permission from Jesse *et. al.*[23] https://doi.org/10.1088/1361-6528/aabb79 © IOP Publishing. All rights reserved). They were able to produce a distinct line of Bi dopants by slowly advancing a linear scan pattern through the crystal. c) A more detailed examination of this phenomenon was performed by Hudak *et al.*,[68] where they were able to gain control of individual Bi atoms within the 3D crystal and assemble the atoms into predetermined patterns. The proposed mechanism of movement involves a two-step process whereby the beam, positioned on a column adjacent to the dopant, creates a vacancy through knock-on damage and inspires the dopant to spontaneously switch columns to fill the vacancy. d) Chuvilin *et al.*,[61] showed how electron beam irradiation could be used to form chains of single carbon atoms from graphene (© Deutsche Physikalische Gesellschaft. Reproduced by permission of IOP Publishing. CC BY-NC-SA, DOI: https://doi.org/10.1088/1367-2630/11/8/083019). e) A similar process was used by Lin *et al.,*[60] to form metallic nanowires in 2D transition-metal dichalcogenides (reprinted from Lin *et al.*[60] 2014, Nature Nanotechnology with permission from Springer Nature). f) Dyck *et al.*,[24] showed how single dopant Si atoms and dimers may be introduced into a graphene lattice through a two-step process: a defect is first created via knock-on damage with the electron beam and then the beam is scanned over the nearby source material to sputter Si atoms toward the defect. As the defect heals it incorporates the dopants into the lattice (reprinted from Dyck *et. al.*[24] 2017, *Applied Physics Letters* with permission from AIP Publishing). g) Susi *et al.*,[27] illustrate how the electron beam can be used to direct Si atoms through the graphene lattice. The proposed mechanism is a sub-threshold impact from an electron on a C atom adjacent to the Si dopant, which inspires a bond inversion (reprinted from Susi *et. al.*[27] 2017, *Ultramicroscopy* with permission from Elsevier). h) Dyck *et al.*,[28] leverage this mechanism to assemble small Si structures, atom-by-atom, within the graphene lattice (reprinted from Dyck *et. al.* 2018, *Small* with permission from John Wiley & Sons).

Several key examples of electron-beam-induced transformations are summarized in Figure 1. There are many examples of beam-induced crystallization (Table 1), but the achievement of controlled crystalline growth of the "ORNL" acronym at the amorphous/crystalline interface in strontium titanate[22] (Figure 1a) demonstrated a high degree of control over the crystallization process; the authors were able to leverage real-time data processing using a custom beam-control interface to create a feedback system and automatically control the beam, which enabled near single atomic layer precision in the crystallization process. This process was then extended[23] to crystallize localized regions of amorphous Si (Figure 1b). In this study, the authors also observed the movement of Bi atoms that had been doped into the Si crystal and showed that the Bi dopants can collectively be directed to form a line through controlled irradiation. This level of control led to renewed interest in further understanding how such processes occur. A more thorough investigation[68] demonstrated that it is possible to direct individual Bi dopants through the Si crystal lattice by careful electron beam placement (Figure 1c), positioning them in a particular atomic column within the Si lattice to obtain Bi patterning and cluster formation. The authors of this study also suggested that controlling the position of the dopants in the third dimension (within an atomic column) might be achievable by tilting the sample to alternate zone axes.

A second set of examples highlights *in situ* nanowire formation through the removal of atoms from a 2D material in TEM and STEM. The formation of one-atom-wide carbon chains from a graphene film through electron beam irradiation was obtained in a TEM[61] (Figure 1d). Similar results have been obtained by other groups[62,88] and extended to other 2D materials; for example, B, N, and BN chains were formed from h-BN,[63] and P chains from black phosphorous.[64] The formation of two atom wide, conducting metallic nanowires from various TMDs was demonstrated,[60] as shown in Figure 1e. These results and others[59,89-91] show that sub-nanometer, conductive flexible wiring within a semiconducting TMD can be achieved in the STEM. It remains to be seen how such capabilities will be leveraged for device fabrication.

Our last set of examples illustrates atomically precise positioning and manipulation of dopant atoms within the graphene lattice. These studies demonstrate that the electron beam can be used to supply energy to a single nanostructure embedded in graphene and change its structure and/or location.[92,93] The natural question is whether the electron probe can be used to *create* such structures. A process for placing Si dopant atoms in a graphene lattice, in which a defect is first created through electron beam exposure and subsequently healed through the incorporation of a Si atom sourced from nearby contaminant material, was developed[24] (Figure 1f). Si dopant atoms can also be directed through the graphene lattice through a bond inversion process[26] induced by targeting neighboring C atoms with the focused probe[27] (Figure 1g). This technique was then leveraged to controllably assemble Si atom clusters, atom-by-atom, in the STEM[28] (Figure 1h).

Physical Mechanisms

Much effort has been put forward to understand electron-beam-induced transformation mechanisms, driven primarily by a desire to mitigate beam damage to the specimen. These effects

can be broadly divided into those brought on by elastic and inelastic electron scattering. With elastic scattering, energy is conserved between the incident electron and the atomic nuclei. This type of energy transfer to the sample results in "knock-on" damage, or atomic displacement (if the energy exceeds some atomic displacement threshold), leading to the generation of vacancies and interstitial defects, dislocation loops,[94] amorphization,[95,96] sputtering,[97] and adatom migration.[98,99] By contrast, inelastic scattering results in the emission of secondary electrons,[100] electrostatic charging in poorly conducting samples, excitation of conductance or valence electrons,[101] atomic ionization, and sample heating. These effects are discussed in several reviews.[14,15,102,103] Here, we are primarily interested in the details of electron-beam-induced atom motion.

The mechanisms underlying these transformations have been studied by optimizing minimum energy reaction pathways and simulating knock-on atomic dynamics in the electronic ground state.[26,27,70,104-108] The results show qualitative agreement with experimentally-observed cross sections for a variety of structural processes in materials. However, the electrons comprising the beam, apart from imparting significant linear momentum to specific knock-on atoms through elastic scattering, also emanate point source electric fields that strongly couple the ground and excited electronic states of materials. EELS and cathodoluminescence techniques both measure the electronic excitations induced in materials through inelastic scattering and demonstrate that the occurrence of significant electronic excitation during TEM and STEM operation is unavoidable. Rapid thermalization of the populations of delocalized conduction band electronic states promotes a homogenous vibrational response to electronic excitation in metallic systems like pristine graphene,[109] but defects in these materials introduce localized electronic states that can exhibit disparate potential energy landscapes relative to the ground state for atoms in the vicinity of the defect.[110] The assumption that electron beam exposure induces a nonequilibrium vibrational

response in materials with no concomitant electronic excitation is not well-justified in general, so an accurate treatment of the electronically non-adiabatic evolution of materials following perturbation by relativistic electrons becomes mandatory for a complete description of beam-induced processes.

The extent to which inelastic scattering effects contribute to cross sections for structural transformations of materials induced by electron beams currently remains unexplored. It is a central tenet in the field of photochemistry, though, that many reactions which cannot be thermally promoted in the electronic ground state due to large free energy barriers can be enacted with high quantum yields through electronic excitation (and, more importantly, the ensuing non-radiative decay processes.)[111-113]

For an electronic excitation to contribute to the mechanism of a structural transformation that preserves the total number of particles of each type (e.g. phase transformations, topological defect formation, defect migration, etc.) it must itself be particle-preserving. It is therefore sufficient to consider just the neutral excitations to bound electronic states of the material when investigating the role of inelastic scattering effects in facilitating transformations of this type. Excited state electronic structure methods such as time-dependent density functional theory (TD-DFT) have been used to calculate the bound electronic states of a material and the coupling between them due to the presence of point source electric fields.[114] The TD-DFT formalism has also be used to propagate the electronic state of the material in "real-time" following perturbation by spatially-localized external charges.[115,116] Non-adiabatic molecular dynamics methods which couple the electronic (TD-DFT) equations of motion and classical vibrational dynamics[117] are also being adopted to study the response of materials to the impact of swift charged particles.[118] Unfortunately, as a single-reference electronic structure method, DFT isn't well-suited for

describing the electronic states of strongly-correlated materials, or the far-from-equilibrium geometries associated with bond breaking and reforming processes,[119,120] suggesting that multi-reference wave function-based methods may ultimately be required for a faithful description of some electron beam-induced phenomena.

In Situ Liquid and Gas Cells

The electron-beam-induced, solid state chemical reactions presented above highlight notable examples of controlled manipulation of dopant atoms that are embedded within a 2D material lattice; however, it is also possible to expand the accessible range of materials by inducing chemical reactions *in situ* directly from a liquid or gas through radiolysis and molecular decomposition of organometallic precursors, respectively. This is accomplished in STEM by (1) encapsulating a liquid- or gas-phase precursor between electron transparent membranes (e.g., silicon nitride, h-BN, or graphene), which are in turn placed within a specialized vacuum-compatible, liquid- or gas-cell TEM holder or (2) using a dedicated environmental TEM (ETEM) that permits the controlled introduction of reactant gases into the sample stage area within the TEM column. The key to inducing the desired material transformations is to utilize a liquid or gas with a reducible chemistry such that site-specific, localized crystallization occurs during the electron beam interactions. The liquid-cell approach relies upon radiolysis, where the highly ionizing radiation imparted by the electron beam will break down water molecules to form reducing radical species, which in turn can chemically reduce metal from a range of organometallic liquid precursor[121] and locally deposit metal in a controlled manner.[79-81,122] By automating the beam control, the ability to directly write high-purity metallic nanostructures from an aqueous solution was demonstrated;[78] this mechanism can also be applied to deposition from organometallic precursor gases.[57,83] With further improvements in understanding and controlling the electron dose

with direct feedback, it may soon be possible to directly transform single and multi-component chemical compounds into functional device architectures with very small feature sizes.

The Role of Feedback

Although these are significant developments, if STEM is to truly become an atomic fabrication platform, such demonstrations must become much more routine. The processes involved in building atomic-scale structures via STEM will require a high degree of automation, which will require instantaneous feedback, exquisite electron beam control and real-time data analysis techniques to obtain, for example, a self-driving microscope that can automatically recognize structures and control the beam to modify them in pre-specified ways. Examples shown in Figure 1a,b illustrate the first steps in this direction, combining feedback, beam control, and real-time data analysis to achieve automated control of the crystalline growth front. In the next section, developments in artificial intelligence that hold promise for creating a self-driving STEM are discussed.

Taken together with the manipulations achievable in STEM, one begins to obtain an exciting picture of what may be possible. The recently suggested "Atomic Forge" concept[13] envisions the STEM as an atomic-scale fabrication platform. Not only does such a platform appear possible, but significant goals in this direction have already been reached.

Advances in Artificial Intelligence for STEM

The real-time image analysis component of active feedback control system for STEM is limited to the analysis of simple structures and physical processes.[23] These control systems rely on the ability to detect crystallinity in the sample, for which the Fourier transform provides a rapid and robust mechanism. However, it is difficult to extend custom-designed methods that address a

specific problem (e.g. crystallinity detection) toward the general case in which, ideally, all material alterations are tracked and structural changes are elucidated automatically. This would enable the use of the beam to manipulate specific atomic groups or particles, and the system would act as a beam-driven robotic device. However, current techniques are not at the level required for the reproducible and automated fabrication of non-trivial 2D and 3D arrays of atomic impurities and defects and for the control of their interactions in an imperfect lattice that may itself undergo changes during a STEM-based manipulation process. Designing new tests for each process or alteration encountered is an intractable problem, as there are innumerable ways in which a sample can be altered. One strategy that may help to circumvent this problem is the use of deep learning techniques[123] for rapid automated analysis of atomically resolved images, which could, in the near term, include real-time reconstruction of the atomic structure (position and type of all the atomic species in the image). In the future, this strategy could conceivably be extended to the automated evaluation of local electronic and magnetic properties of the system through the use of libraries of theoretical calculations. This approach provides the level of abstraction necessary to begin generalizing solutions to the problem of extracting useful information from data in an automated fashion. This abstraction is, of course, precisely why there is such intense interest in artificial intelligence. Deep-learning-based image analysis has been successfully used in various areas of science and engineering, ranging from cancer detection[124] to satellite imaging,[125] but it has only recently been applied to the analysis of atomically resolved STEM images.

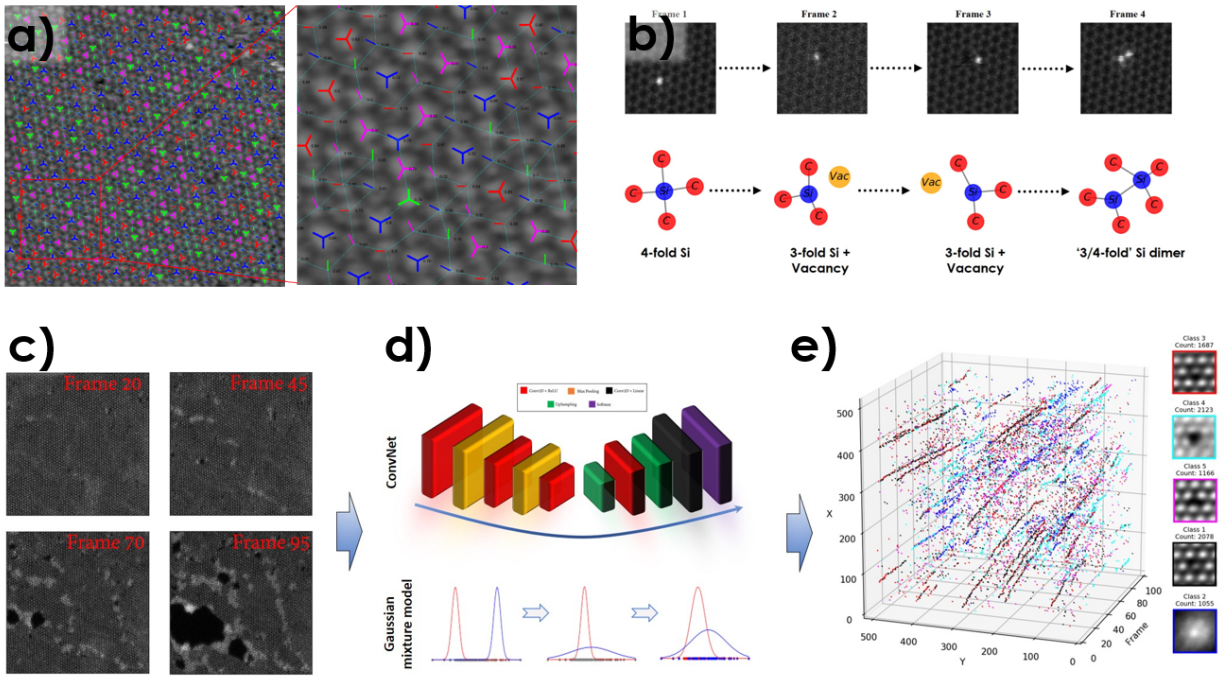

Figure 2 Applications of deep convolutional neural networks (DCNN) to atomic-scale image analysis. a) Ziatdinov *et al.*,[126] use theoretical simulations to train a DCNN to automatically recognize molecular orientations from scanning tunneling microscopy images (adapted from Ziatdinov *et al.*[126] npj Computational Materials 3, 31 (2017) under the Creative Commons license http://creativecommons.org/licenses/by/4.0/). b) Ziatdinov *et al.*,[127] use a DCNN to recognize the structural evolution of atomic clusters in graphene (Reprinted with permission from Ziatdinov *et al.*[126] *ACS Nano* 11, 12742 (2017) Copyright (2017) American Chemical Society). c) Maksov *et al.*[128] use a combination of deep learning and unsupervised unmixing techniques to identify, classify, and track electron beam-induced defects in STEM movies. Shown is the material evolution through time. d) Schematics of machine learning analysis of the data where DCNNs (upper panel) are first used to locate atomic defects in the raw experimental data and then a Gaussian mixture model (lower panel) is applied to the extracted defect structures (set of sub-images centered around each defect) to categorize them into different classes. e) The 3D representation shows each detected defect x/y position and frame number color coded according to defect type – it is clear that a "by hand" analysis is completely impractical given the tremendous number of defects present. (c)-(e) adapted from Maksov *et al.*[128] *npj Computational Materials* **5**, 12 (2019) under the Creative Commons license http://creativecommons.org/licenses/by/4.0/.

Examples of deep-learning-based image analysis are shown in Figure 2. Deep convolutional neural networks (DCNN) trained on DFT-calculated data in combination with Markov random field modelling were successfully applied to the analysis of molecular orientations in STM images[126] (Figure 2a). It was then demonstrated that DCNNs can be used to identify the position of atoms, atomic columns, and different types of lattice defects in atomically resolved STEM images[127,129] (Figure 2b). The use of DCNNs for automatic determination of the Bravais lattice symmetry in atomically resolved STEM images was also reported[130]. In all these cases, a deep learning model trained using simulated STEM data was able to successfully generalize to

previously unseen noisy experimental data. Just as important, the speed of image processing on a trained network should allow the implementation of the deep-learning-based analysis of STEM experiments in real time, though this has yet to be demonstrated. Because the training sets for DCNNs are generated from a known physical model (such as the Multi-slice algorithm[131]), various physical constraints are implicitly included in the deep learning model.

It is also possible to analyze the movement and alterations of lattice point defects in STEM movies using a combination of a deep learning model trained on a single (first) frame of an experimental movie and unsupervised (with no prior information about the structures) unmixing techniques[128]. In the example summarized in Figure 2 c)-e), a video of electron beam-induced degradation of WS_2 was analyzed. The evolution of the WS_2 structural changes with electron beam exposure time are shown in the STEM images in Figure 2c. Plotting the spatial position and frame number of each detected defect results in the 3D scatterplot in Figure 2e. The large number of datapoints illustrates the challenge that this type of analysis would present if it were to be undertaken "by hand" as well as the rich material dynamics, which would be difficult to capture. The conceptual strategy behind this approach is shown in Figure 2d: the top panel shows the DCNN layers represented schematically in an encoder-decoder structure (a SegNet-like architecture[132]) used for pixel-wise image classification. The encoder consists of convolutional layers for feature extraction (red) and max-pooling (orange) to account for translational invariance and reduce the data size. The decoder maps the low-resolution features produced by the encoder to full-resolution feature maps through application of convolutional layers (red) with the same number of filters as in the encoder and an upsampling operation (green). Finally, a softmax classifier (purple) is used to calculate the probability for each pixel to be a defect. In the lower panel, a simplified schematic description of a Gaussian mixture model is shown. The

Gaussian mixture model categorizes the extracted features (partitions them into "clusters") by searching for a finite number of Gaussian distributions (e.g. red and blue curves) that can model the data. In this example, the Gaussian curves are shown at three steps during the convergence process.

Although these examples demonstrate how a machine learning approach can be used to automate data analysis, it remains to be seen which and how many problems lend themselves to being solved using this approach. One potential disadvantage of approaches based on deep learning is the lack of problem-specific (and physics-based) methods for choosing the model hyperparameters that specify how the network will behave. Presently, choosing the hyperparameters involves a large degree of manual fine tuning and it is often unclear for a non-expert (and sometimes even for experts) how the network hyperparameters should be optimized for a particular problem. It is therefore critical to develop a procedure guided by the physics of the problem that can optimally and quickly examine the large hyperparameter space and converge on a deep learning model that is best suited to the physical problem at hand.

Perspectives: The advances in aberration correction have enabled STEM imaging at voltages well below the knock-on threshold for many materials. In this low-voltage regime, the electron beam can induce a broad range of chemical and physical processes ranging from the movement of dopant atoms and formation of vacancies to the making and breaking of chemical bonds. The relatively low effective cross-sections for some of these processes enable the separation of STEM imaging and manipulation modes; multiple STEM images can be acquired between the manipulation events, allowing for human-based feedback for the creation of predefined structures. Advances in machine learning and big data techniques hold promise for rapid acceleration of the process

through the introduction of compressed sensing methods for imaging at lower effective doses and implementation of real time feedback, opening a pathway for atomic manipulation and transforming the STEM into a tool for atom-by-atom fabrication of nanostructures.

This discussion also illustrates the importance of the microscope operating conditions used, such as beam current or accelerating voltage. For many of the examples reviewed here, the same beam conditions were used to both image materials and manipulate them, leading to some level of unwanted structural alterations. In an ideal STEM it would be possible to rapidly switch beam energy (or current) as needed for different modes of operation. The power of this strategy was demonstrated by inserting dopants in a graphene lattice using a 100 kV beam and switching to a 60 kV beam to manipulate the dopants and assemble structures[28]. Unfortunately, changing the microscope voltage typically requires several hours for the microscope to stabilize, making variable electron energy experiments prohibitively time consuming. The primary cause of the lengthy wait for microscope stability is the change in temperature of the microscope lenses at different power settings. Strategies for maintaining a constant temperature are under development and should enable more rapid voltage changes, with significant benefits for general microscope operation, as well as for this field of atomic manipulation.

A second consideration regarding STEM imaging and manipulation modes lies in defining their purpose. Specifically, imaging is used to observe the material's structure, to detect any alterations in the structure, and to inform about what process should be induced next during manipulation. Alternatively, signals generated *during* manipulation may be leveraged to produce information about the sample state, removing the need for continuous imaging, which exposes the sample to excess irradiation and may negatively alter the specimen and the structure being fabricated. One example of such a strategy was the use of real-time analysis and feedback to gain automated control

of a crystal growth front in STEM[22] (Figure 1a). Fourier transforms of each scan line performed during manipulation were used to determine the degree of local crystallinity in the sample. In this way, no image of the crystallization progress was required to establish atomic-level control over the growth process, which was achieved by automatically adjusting the beam position and electron dose in response to the sample state. Present day STEMs may be equipped with a range of modalities, including EELS, EDS, diffraction, convergent beam electron diffraction or 4D STEM, cathodoluminescence, and annular dark field imaging, which all have the capability of producing localized information from a single beam position on the sample. Harnessing and integrating these capabilities during manipulation to gain sample information without needing to form a whole image at each position will greatly enhance the speed and accuracy of manipulation by preventing unnecessary irradiation and unintended alterations. A parallel development in imaging also holds promise for reducing unintended structural alterations: compressed sensing or sparse sampling can be used to reduce the radiation dose. Although feedback remains extremely important, even when unwanted changes occur, as long as it is possible to detect and correct them relatively quickly, progress toward the desired structure is still possible.

Concurrent with the development of STEM imaging and manipulation modes with their respective data-generating schema, there must also exist ways to automatically extract *knowledge* about the sample from the data. Returning to the previous example of controlled beam-induced crystallization[22], the authors were able to extract a measure of the degree of crystallinity of the crystal growth front and induce an automated response to this knowledge. In a similar way, additional tools must be developed to process the data and extract knowledge about the sample so that automated microscope responses can be programmed. The generalizability of machine learning, as described previously, suggests that it is well suited for such knowledge extraction.

However, machine learning techniques rely on training datasets, which must be generated beforehand. Thus, a significant effort toward building useful libraries of structures, simulations, and images for training, real-time comparison and interpretation of data is pivotal for the implementation of this strategy.

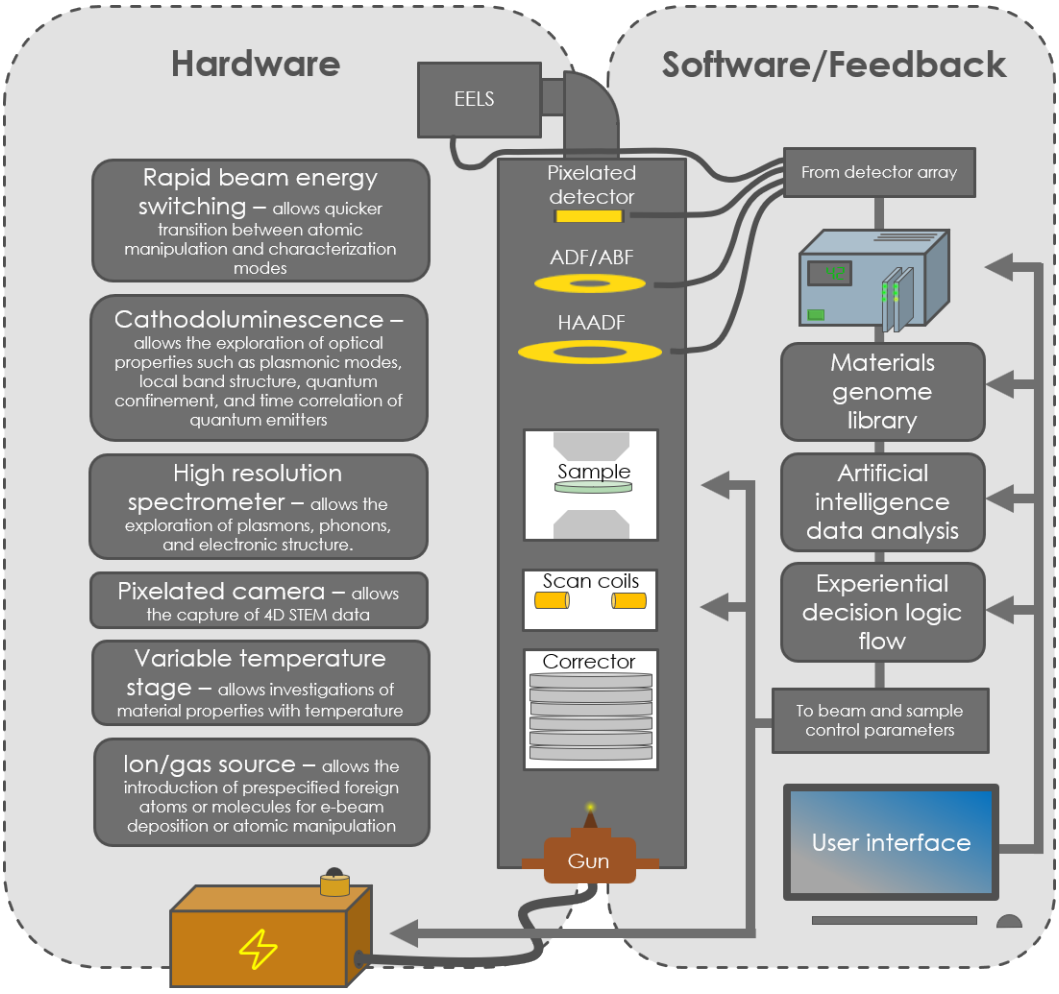

Figure 3 Conceptual schematic of a modern STEM updated to operate as an Atom Forge. On the hardware side we highlight a number of advancements that will enhance the STEM characterization capabilities, particularly with respect to the detection of quantum phenomenon when integrated into a single platform. On the software/feedback side we illustrate an advanced data acquisition and control module, which receives signals from the detector array installed on the microscope, interfaces with the user workstation, and leverages a materials genome-type library of information. Artificial intelligence-driven real-time data analysis will process the data to extract useful information about the sample state and use prior experience (learned on its own or programmed in) to decide on appropriate microscope action to alter the sample toward a prespecified atomic configuration.

A conceptual diagram of a STEM turned into an Atom Forge, purpose built for atomic fabrication, is shown in Figure 3. The two main categories of development, hardware and

software/feedback, are shown on either side of the microscope. We have already discussed software/feedback using automated crystallization as an example and suggested that more general feedback solutions could be constructed by leveraging artificial intelligence.

On the hardware side, the integration of key capabilities for the detection and characterization of quantum phenomena is needed. In particular, to generate local information from a stationary, positioned beam, diffraction data can be acquired, leveraging rapid acquisition pixelated detectors. A high-energy-resolution spectrometer would enable unique insight into low energy transitions such as phonon and plasmon modes. Ultimately, this type of instrument should enable the measurement of spin and orbital ordering of individual atoms or atomic scale qubits.

Finally, in the effort toward atom-by-atom fabrication, it is important to define significant milestones. Although many valid measurements of progress can be devised, for simplicity we choose fabrication complexity and lay out a roadmap of milestones with increasing complexity for 2D and 3D materials (Figure 4). For 3D materials we have sculpting in 2D (i.e., only in the x and y directions),[22] manipulation of single dopants in 2D,[68] sculpting in 3D, atom movement in 3D, 3D assembly, and device fabrication. For 2D materials, we have isolating single atoms (placing atoms in the lattice),[24] moving single atoms,[27] assembling homo-atomic structures,[28] assembling hetero-atomic structures, assembling functionalized structures, and device fabrication. While this is certainly not a comprehensive set of possible milestones, they will serve as a rough indication of the state of progress. It is exciting to note the number of milestones that have already been reached.

Overall, since its inception, electron microscopy was perceived predominantly as a tool to visualize atomic structure. Roughly twenty years after the advent of the aberration corrector, we observe its evolution toward a machine capable of manipulating atomic structures, visualizing

them with picometer precision, and inferring their physical properties, ranging from electronic and phononic to quantum mechanical properties.

Acknowledgements

Work was supported by the Laboratory Directed Research and Development Program of Oak Ridge National Laboratory, managed by UT-Battelle, LLC for the U.S. Department of Energy (O.D., M.Z., S.J.), Oak Ridge National Laboratory's Center for Nanophase Materials Sciences (CNMS), a U.S. Department of Energy Office of Science User Facility (D.L. R.R.U., S.V.K.), and the U.S. Department of Energy, Office of Science, Basic Energy Sciences, Division of Materials Science and Engineering (B.M.H., A.R.L.).

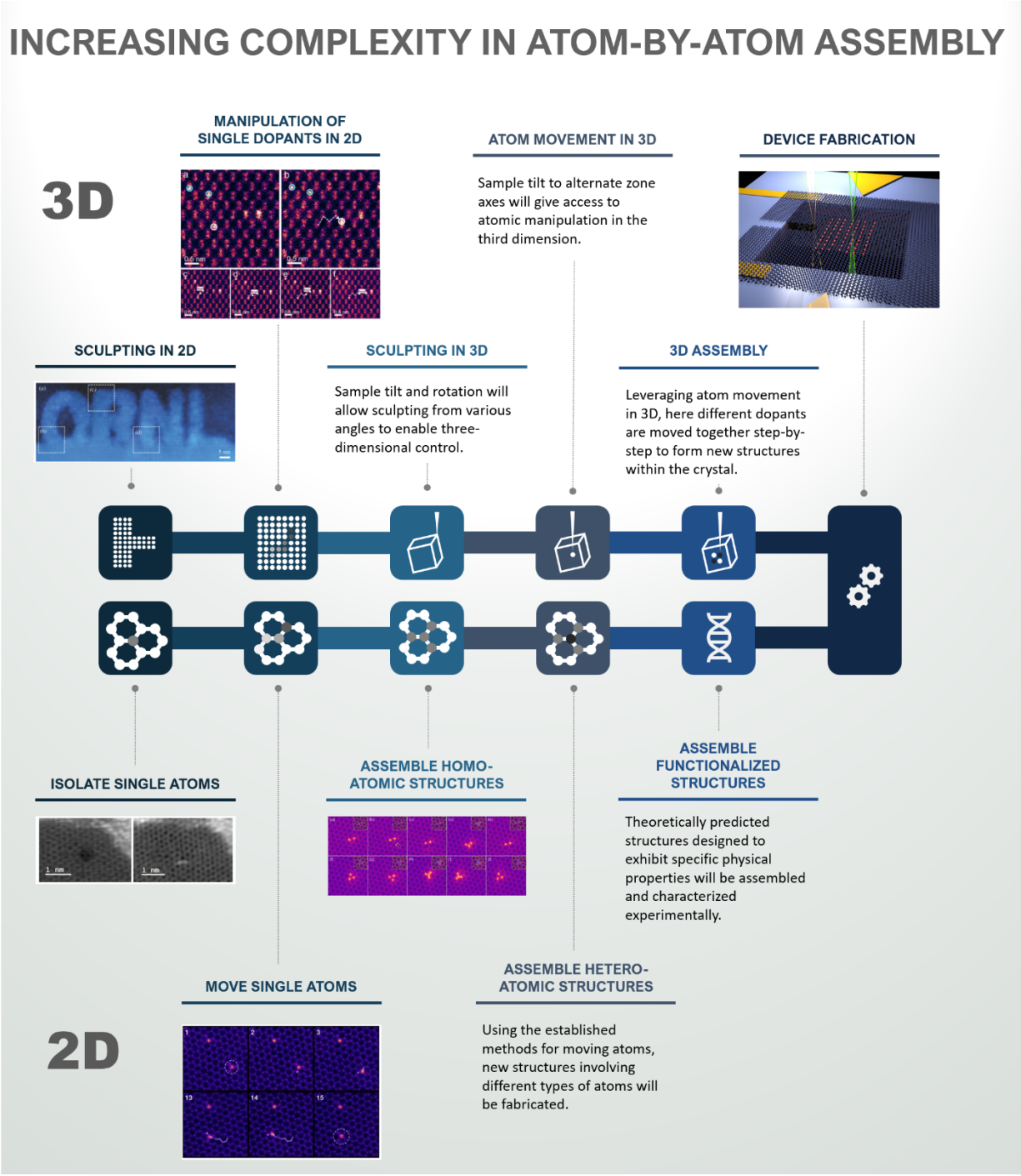

Figure 4 Schematic of the increasingly complex milestone demonstrations on the road toward atom-by-atom device fabrication. Demonstrations with images (except for the image depicting device fabrication) have already been accomplished. The top half details the complexity of milestones to be accomplished in 3D materials while the bottom half details the complexity of milestones to be accomplished in 2D materials. The shared goal is, finally, to demonstrate the atom-by-atom manufacture of functional devices illustrated by the artist's rendering of an emitter array being constructed in graphene using e-beams.

References

1 Feynman, R. P. There's plenty of room at the bottom. *Engineering and science* **23**, 22-36 (1960).

2 Eigler, D. M. & Schweizer, E. K. Positioning single atoms with a scanning tunnelling microscope. *Nature* **344**, 524-526 (1990).

3 Fuechsle, M. *et al.* A single-atom transistor. *Nat Nano* **7**, 242-246 (2012).

4 Huff, T. *et al.* Binary atomic silicon logic. *Nature Electronics* **1**, 636-643, doi:10.1038/s41928-018-0180-3 (2018).

5 Oyabu, N., Custance, Ó., Yi, I., Sugawara, Y. & Morita, S. Mechanical Vertical Manipulation of Selected Single Atoms by Soft Nanoindentation Using Near Contact Atomic Force Microscopy. *Phys. Rev. Lett.* **90**, 176102, doi:10.1103/PhysRevLett.90.176102 (2003).

6 Sugimoto, Y. *et al.* Atom inlays performed at room temperature using atomic force microscopy. *Nat. Mater.* **4**, 156, doi:10.1038/nmat1297

https://www.nature.com/articles/nmat1297#supplementary-information (2005).

7 Sugimoto, Y. *et al.* Complex Patterning by Vertical Interchange Atom Manipulation Using Atomic Force Microscopy. *Science* **322**, 413-417, doi:10.1126/science.1160601 (2008).

8 Sugimoto, Y., Yurtsever, A., Hirayama, N., Abe, M. & Morita, S. Mechanical gate control for atom-by-atom cluster assembly with scanning probe microscopy. *Nat. Commun.* **5**, 4360, doi:10.1038/ncomms5360

https://www.nature.com/articles/ncomms5360#supplementary-information (2014).

9 Yamazaki, S. *et al.* Interplay between Switching Driven by the Tunneling Current and Atomic Force of a Bistable Four-Atom Si Quantum Dot. *Nano Lett.* **15**, 4356-4363, doi:10.1021/acs.nanolett.5b00448 (2015).

10 Drexler, E. K. Engines of creation: the coming era of nanotechnology. *Anchor Book* (1986).

11 Drexler, E. K. *Nanosystems: molecular machinery, manufacturing, and computation.[1](1991)*. (Univ., 1991).

12 *The Nobel Prize in Chemistry 2016*, <http://www.nobelprize.org/nobel_prizes/chemistry/laureates/2016/> (2014).

13 Kalinin, S. V., Borisevich, A. & Jesse, S. Fire up the atom forge. *Nature* **539**, 485-487 (2016).

14 Egerton, R. F., Li, P. & Malac, M. Radiation damage in the TEM and SEM. *Micron* **35**, 399-409, doi:http://dx.doi.org/10.1016/j.micron.2004.02.003 (2004).

15 Jiang, N. Electron beam damage in oxides: a review. *Rep. Prog. Phys.* **79**, 016501 (2016).

16 Yankovich, A. B. *et al.* Picometre-precision analysis of scanning transmission electron microscopy images of platinum nanocatalysts. *Nat Commun* **5**, 4155, doi:10.1038/ncomms5155 (2014).

17 Sang, X. & LeBeau, J. M. Revolving scanning transmission electron microscopy: Correcting sample drift distortion without prior knowledge. *Ultramicroscopy* **138**, 28-35, doi:http://dx.doi.org/10.1016/j.ultramic.2013.12.004 (2014).

18 Kimoto, K. *et al.* Local crystal structure analysis with several picometer precision using scanning transmission electron microscopy. *Ultramicroscopy* **110**, 778-782, doi:http://dx.doi.org/10.1016/j.ultramic.2009.11.014 (2010).

19 Jang, J. H. *et al.* In Situ Observation of Oxygen Vacancy Dynamics and Ordering in the Epitaxial LaCoO3 System. *ACS Nano* **11**, 6942-6949, doi:10.1021/acsnano.7b02188 (2017).

20 Kotakoski, J., Mangler, C. & Meyer, J. C. Imaging atomic-level random walk of a point defect in graphene. *Nat. Commun.* **5**, 3991, doi:10.1038/ncomms4991

https://www.nature.com/articles/ncomms4991#supplementary-information (2014).

21 Ishikawa, R. *et al.* Direct Observation of Dopant Atom Diffusion in a Bulk Semiconductor Crystal Enhanced by a Large Size Mismatch. *Phys. Rev. Lett.* **113**, 155501 (2014).

22 Jesse, S. *et al.* Atomic-Level Sculpting of Crystalline Oxides: Toward Bulk Nanofabrication with Single Atomic Plane Precision. *Small* **11**, 5895-5900, doi:10.1002/smll.201502048 (2015).

23 Jesse, S. *et al.* Direct atomic fabrication and dopant positioning in Si using electron beams with active real-time image-based feedback. *Nanotechnology* **29**, 255303 (2018).

24 Dyck, O., Kim, S., Kalinin, S. V. & Jesse, S. Placing single atoms in graphene with a scanning transmission electron microscope. *Appl. Phys. Lett.* **111**, 113104, doi:10.1063/1.4998599 (2017).

25 Tripathi, M. *et al.* Electron-Beam Manipulation of Silicon Dopants in Graphene. *Nano Lett.*, doi:10.1021/acs.nanolett.8b02406 (2018).

26 Susi, T. *et al.* Silicon-Carbon Bond Inversions Driven by 60-keV Electrons in Graphene. *Phys. Rev. Lett.* **113**, 115501 (2014).

27 Susi, T., Meyer, J. C. & Kotakoski, J. Manipulating low-dimensional materials down to the level of single atoms with electron irradiation. *Ultramicroscopy* **180**, 163-172, doi:http://dx.doi.org/10.1016/j.ultramic.2017.03.005 (2017).

28 Dyck, O. *et al.* Building Structures Atom by Atom via Electron Beam Manipulation. *Small* **14**, 1801771, doi:doi:10.1002/smll.201801771 (2018).

29 Pennycook, S. J. & Nellist, P. D. (Springer, New York, 2011).

30 Scherzer, O. The Theoretical Resolution Limit of the Electron Microscope. *J. Appl. Phys.* **20**, 20-29, doi:10.1063/1.1698233 (1949).

31 Pennycook, S. J. & Nellist, P. D. *Scanning transmission electron microscopy: imaging and analysis*. (Springer Science & Business Media, 2011).

32 Sawada, H. *et al.* STEM imaging of 47-pm-separated atomic columns by a spherical aberration-corrected electron microscope with a 300-kV cold field emission gun. *J. Electron Microsc.* **58**, 357-361, doi:10.1093/jmicro/dfp030 (2009).

33 Erni, R., Rossell, M. D., Kisielowski, C. & Dahmen, U. Atomic-Resolution Imaging with a Sub-50-pm Electron Probe. *Phys. Rev. Lett.* **102**, 096101, doi:10.1103/PhysRevLett.102.096101 (2009).

34 Hawkes, P. W. The correction of electron lens aberrations. *Ultramicroscopy* **156**, A1-A64, doi:https://doi.org/10.1016/j.ultramic.2015.03.007 (2015).

35 Hawkes, P. W. *Advances in Imaging and Electron Physics: Aberration-corrected Electron Microscopy*. (Elsevier Science, 2009).

36 Orloff, J. *Handbook of Charged Particle Optics, Second Edition*. (CRC Press, 2008).

37 Haider, M. *et al.* Electron microscopy image enhanced. *Nature* **392**, 768, doi:10.1038/33823 (1998).

38 Krivanek, O. L., Dellby, N. & Lupini, A. R. Towards sub-Å electron beams. *Ultramicroscopy* **78**, 1-11, doi:http://dx.doi.org/10.1016/S0304-3991(99)00013-3 (1999).

39 Dellby, N., Krivanek, L., Nellist, D., Batson, E. & Lupini, R. Progress in aberration-corrected scanning transmission electron microscopy. *J. Electron Microsc.* **50**, 177-185, doi:10.1093/jmicro/50.3.177 (2001).

40 Novoselov, K. S. *et al.* Electric Field Effect in Atomically Thin Carbon Films. *Science* **306**, 666-669, doi:10.1126/science.1102896 (2004).

41 Novoselov, K. S. *et al.* Two-dimensional atomic crystals. *Proc. Natl. Acad. Sci. U.S.A.* **102**, 10451-10453, doi:10.1073/pnas.0502848102 (2005).

42 Geim, A. K. & Novoselov, K. S. The rise of graphene. *Nat. Mater.* **6**, 183, doi:10.1038/nmat1849 (2007).

43 Song, L. *et al.* Large Scale Growth and Characterization of Atomic Hexagonal Boron Nitride Layers. *Nano Lett.* **10**, 3209-3215, doi:10.1021/nl1022139 (2010).

44 Chhowalla, M., Liu, Z. & Zhang, H. Two-dimensional transition metal dichalcogenide (TMD) nanosheets. *Chem. Soc. Rev.* **44**, 2584-2586 (2015).
45 Liu, H. *et al.* Phosphorene: An Unexplored 2D Semiconductor with a High Hole Mobility. *ACS Nano* **8**, 4033-4041, doi:10.1021/nn501226z (2014).
46 Martin, P. & Zdeněk, S. 2D Monoelemental Arsenene, Antimonene, and Bismuthene: Beyond Black Phosphorus. *Adv. Mater.* **29**, 1605299, doi:doi:10.1002/adma.201605299 (2017).
47 Lalmi, B. *et al.* Epitaxial growth of a silicene sheet. *Appl. Phys. Lett.* **97**, 223109, doi:10.1063/1.3524215 (2010).
48 Dávila, M. E., Xian, L., Cahangirov, S., Rubio, A. & Lay, G. L. Germanene: a novel two-dimensional germanium allotrope akin to graphene and silicene. *New Journal of Physics* **16**, 095002 (2014).
49 Zhao, J. *et al.* Free-Standing Single-Atom-Thick Iron Membranes Suspended in Graphene Pores. *Science* **343**, 1228-1232, doi:10.1126/science.1245273 (2014).
50 Quang, H. T. *et al.* In Situ Observations of Free-Standing Graphene-like Mono- and Bilayer ZnO Membranes. *ACS Nano* **9**, 11408-11413, doi:10.1021/acsnano.5b05481 (2015).
51 Xiaoxu, Z. *et al.* Atom-by-Atom Fabrication of Monolayer Molybdenum Membranes. *Adv. Mater.* **0**, 1707281, doi:doi:10.1002/adma.201707281 (2018).
52 Michael, N. *et al.* Two-Dimensional Nanocrystals Produced by Exfoliation of Ti3AlC2. *Adv. Mater.* **23**, 4248-4253, doi:doi:10.1002/adma.201102306 (2011).
53 Krivanek, O. L. *et al.* Atom-by-atom structural and chemical analysis by annular dark-field electron microscopy. *Nature* **464**, 571-574, doi:http://www.nature.com/nature/journal/v464/n7288/suppinfo/nature08879_S1.html (2010).
54 LeBeau, J. M., Findlay, S. D., Allen, L. J. & Stemmer, S. Quantitative Atomic Resolution Scanning Transmission Electron Microscopy. *Phys. Rev. Lett.* **100**, 206101 (2008).
55 Hwang, J., Zhang, J. Y., D'Alfonso, A. J., Allen, L. J. & Stemmer, S. Three-Dimensional Imaging of Individual Dopant Atoms in SrTiO3. *Phys. Rev. Lett.* **111**, 266101, doi:10.1103/PhysRevLett.111.266101 (2013).
56 Wei, X., Wang, M.-S., Bando, Y. & Golberg, D. Electron-Beam-Induced Substitutional Carbon Doping of Boron Nitride Nanosheets, Nanoribbons, and Nanotubes. *ACS Nano* **5**, 2916-2922, doi:10.1021/nn103548r (2011).
57 Dorp, W. F. v. *et al.* Nanometer-scale lithography on microscopically clean graphene. *Nanotechnology* **22**, 505303 (2011).
58 Fischbein, M. D. & Drndić, M. Sub-10 nm Device Fabrication in a Transmission Electron Microscope. *Nano Lett.* **7**, 1329-1337, doi:10.1021/nl0703626 (2007).
59 Liu, X. *et al.* Top–down fabrication of sub-nanometre semiconducting nanoribbons derived from molybdenum disulfide sheets. *Nat. Commun.* **4**, 1776, doi:10.1038/ncomms2803

https://www.nature.com/articles/ncomms2803#supplementary-information (2013).
60 Lin, J. *et al.* Flexible metallic nanowires with self-adaptive contacts to semiconducting transition-metal dichalcogenide monolayers. *Nature Nanotechnology* **9**, 436, doi:10.1038/nnano.2014.81

https://www.nature.com/articles/nnano.2014.81#supplementary-information (2014).
61 Chuvilin, A., Meyer, J. C., Algara-Siller, G. & Kaiser, U. From graphene constrictions to single carbon chains. *New Journal of Physics* **11**, 083019 (2009).
62 Jin, C., Lan, H., Peng, L., Suenaga, K. & Iijima, S. Deriving Carbon Atomic Chains from Graphene. *Phys. Rev. Lett.* **102**, 205501, doi:10.1103/PhysRevLett.102.205501 (2009).
63 Cretu, O. *et al.* Experimental Observation of Boron Nitride Chains. *ACS Nano* **8**, 11950-11957, doi:10.1021/nn5046147 (2014).

64 Xiao, Z. *et al.* Deriving phosphorus atomic chains from few-layer black phosphorus. *Nano Research* **10**, 2519-2526, doi:10.1007/s12274-017-1456-z (2017).
65 Kondo, Y. & Takayanagi, K. Gold Nanobridge Stabilized by Surface Structure. *Phys. Rev. Lett.* **79**, 3455-3458, doi:10.1103/PhysRevLett.79.3455 (1997).
66 Fischbein, M. D. & Drndić, M. Electron beam nanosculpting of suspended graphene sheets. *Appl. Phys. Lett.* **93**, 113107, doi:10.1063/1.2980518 (2008).
67 Song, B. *et al.* Atomic-Scale Electron-Beam Sculpting of Near-Defect-Free Graphene Nanostructures. *Nano Lett.* **11**, 2247-2250, doi:10.1021/nl200369r (2011).
68 Hudak, B. M. *et al.* Directed Atom-by-Atom Assembly of Dopants in Silicon. *ACS Nano*, doi:10.1021/acsnano.8b02001 (2018).
69 Dyck, O., Kim, S., Kalinin, S. V. & Jesse, S. E-beam manipulation of Si atoms on graphene edges with an aberration-corrected scanning transmission electron microscope. *Nano Research*, doi:10.1007/s12274-018-2141-6 (2018).
70 Su, C. *et al.* Competing dynamics of single phosphorus dopant in graphene with electron irradiation. *ArXiv e-prints* (2018).
71 Jenčič, I., Bench, M. W., Robertson, I. M. & Kirk, M. A. Electron-beam-induced crystallization of isolated amorphous regions in Si, Ge, GaP, and GaAs. *J. Appl. Phys.* **78**, 974-982, doi:10.1063/1.360764 (1995).
72 Bae, I.-T., Zhang, Y., Weber, W. J., Higuchi, M. & Giannuzzi, L. A. Electron-beam induced recrystallization in amorphous apatite. *Appl. Phys. Lett.* **90**, 021912, doi:10.1063/1.2430779 (2007).
73 Jenčič, I., Robertson, I. M. & Skvarč, J. Electron beam induced regrowth of ion implantation damage in Si and Ge. *Nuclear Instruments and Methods in Physics Research Section B: Beam Interactions with Materials and Atoms* **148**, 345-349, doi:https://doi.org/10.1016/S0168-583X(98)00781-2 (1999).
74 Becerril, M. *et al.* Crystallization from amorphous structure to hexagonal quantum dots induced by an electron beam on CdTe thin films. *J. Cryst. Growth* **311**, 1245-1249, doi:https://doi.org/10.1016/j.jcrysgro.2008.12.056 (2009).
75 Yang, X., Wang, R., Yan, H. & Zhang, Z. Low energy electron-beam-induced recrystallization of continuous GaAs amorphous foils. *Materials Science and Engineering: B* **49**, 5-13, doi:https://doi.org/10.1016/S0921-5107(97)00104-9 (1997).
76 Xu, Z. W. & Ngan †, A. H. W. TEM study of electron beam-induced crystallization of amorphous GeSi films. *Philos. Mag. Lett.* **84**, 719-728, doi:10.1080/14786430500038088 (2004).
77 Matsuda, J., Yoshida, K., Sasaki, Y., Uchiyama, N. & Akiba, E. In situ observation on hydrogenation of Mg-Ni films using environmental transmission electron microscope with aberration correction. *Appl. Phys. Lett.* **105**, 083903, doi:10.1063/1.4894101 (2014).
78 Unocic, R. R. *et al.* Direct-write liquid phase transformations with a scanning transmission electron microscope. *Nanoscale* **8**, 15581-15588, doi:10.1039/C6NR04994J (2016).
79 Yin, L., Xin, C., Kyong Wook, N. & Shen, J. D. Electron beam induced deposition of silicon nanostructures from a liquid phase precursor. *Nanotechnology* **23**, 385302 (2012).
80 Donev, E. U., Schardein, G., Wright, J. C. & Hastings, J. T. Substrate effects on the electron-beam-induced deposition of platinum from a liquid precursor. *Nanoscale* **3**, 2709-2717, doi:10.1039/C1NR10026B (2011).
81 Put, M. W. P. v. d. *et al.* Writing Silica Structures in Liquid with Scanning Transmission Electron Microscopy. *Small* **11**, 585-590, doi:doi:10.1002/smll.201400913 (2015).
82 Shimojo, M., Mitsuishi, K., Tameike, A. & Furuya, K. Electron induced nanodeposition of tungsten using field emission scanning and transmission electron microscopes. *Journal of Vacuum Science*

& Technology B: Microelectronics and Nanometer Structures Processing, Measurement, and Phenomena **22**, 742-746, doi:10.1116/1.1688349 (2004).

83 van Dorp, W. F. *et al.* Molecule-by-Molecule Writing Using a Focused Electron Beam. *ACS Nano* **6**, 10076-10081, doi:10.1021/nn303793w (2012).

84 Dyck, O., Kim, S., Kalinin, S. V. & Jesse, S. Mitigating e-beam-induced hydrocarbon deposition on graphene for atomic-scale scanning transmission electron microscopy studies. *J. Vac. Sci. Technol., B: Nanotechnol. Microelectron.: Mater., Process., Meas., Phenom.* **36**, 011801, doi:10.1116/1.5003034 (2017).

85 Lin, Y.-C., Dumcenco, D. O., Huang, Y.-S. & Suenaga, K. Atomic mechanism of the semiconducting-to-metallic phase transition in single-layered MoS2. *Nature Nanotechnology* **9**, 391, doi:10.1038/nnano.2014.64

https://www.nature.com/articles/nnano.2014.64#supplementary-information (2014).

86 Vicarelli, L., Heerema, S. J., Dekker, C. & Zandbergen, H. W. Controlling Defects in Graphene for Optimizing the Electrical Properties of Graphene Nanodevices. *ACS Nano* **9**, 3428-3435, doi:10.1021/acsnano.5b01762 (2015).

87 Kotakoski, J. *et al.* Stone-Wales-type transformations in carbon nanostructures driven by electron irradiation. *Phys. Rev. B* **83**, 245420 (2011).

88 Lin, Y.-C. *et al.* Unexpected Huge Dimerization Ratio in One-Dimensional Carbon Atomic Chains. *Nano Lett.* **17**, 494-500, doi:10.1021/acs.nanolett.6b04534 (2017).

89 Lehtinen, O. *et al.* Atomic Scale Microstructure and Properties of Se-Deficient Two-Dimensional MoSe2. *ACS Nano* **9**, 3274-3283, doi:10.1021/acsnano.5b00410 (2015).

90 Lin, J., Zhang, Y., Zhou, W. & Pantelides, S. T. Structural Flexibility and Alloying in Ultrathin Transition-Metal Chalcogenide Nanowires. *ACS Nano* **10**, 2782-2790, doi:10.1021/acsnano.5b07888 (2016).

91 Koh, A. L. *et al.* Torsional Deformations in Subnanometer MoS Interconnecting Wires. *Nano Lett.* **16**, 1210-1217, doi:10.1021/acs.nanolett.5b04507 (2016).

92 Lee, J., Zhou, W., Pennycook, S. J., Idrobo, J.-C. & Pantelides, S. T. Direct visualization of reversible dynamics in a Si6 cluster embedded in a graphene pore. **4**, 1650, doi:10.1038/ncomms2671

https://www.nature.com/articles/ncomms2671#supplementary-information (2013).

93 Yang, Z. *et al.* Direct Observation of Atomic Dynamics and Silicon Doping at a Topological Defect in Graphene. *Angew. Chem.* **126**, 9054-9058, doi:10.1002/ange.201403382 (2014).

94 King, W. E., Benedek, R., Merkle, K. L. & Meshii, M. Damage effects of high energy electrons on metals. *Ultramicroscopy* **23**, 345-353, doi:https://doi.org/10.1016/0304-3991(87)90245-2 (1987).

95 Hobbs, L. W. The role of topology and geometry in the irradiation-induced amorphization of network structures. *J. Non-Cryst. Solids* **182**, 27-39, doi:https://doi.org/10.1016/0022-3093(94)00574-5 (1995).

96 Hobbs, L. W., Clinard, F. W., Zinkle, S. J. & Ewing, R. C. Radiation effects in ceramics. *J. Nucl. Mater.* **216**, 291-321, doi:https://doi.org/10.1016/0022-3115(94)90017-5 (1994).

97 Bradley, C. R. & Zaluzec, N. J. Atomic sputtering in the Analytical Electron Microscope. *Ultramicroscopy* **28**, 335-338, doi:https://doi.org/10.1016/0304-3991(89)90320-3 (1989).

98 Egerton, R. F. Beam-Induced Motion of Adatoms in the Transmission Electron Microscope. *Microsc. Microanal.* **19**, 479-486, doi:10.1017/S1431927612014274 (2013).

99 Egerton, R. F. & Watanabe, M. Characterization of single-atom catalysts by EELS and EDX spectroscopy. *Ultramicroscopy* **193**, 111-117, doi:https://doi.org/10.1016/j.ultramic.2018.06.013 (2018).

100 Wu, B. & Neureuther, A. R. Energy deposition and transfer in electron-beam lithography. *Journal of Vacuum Science & Technology B: Microelectronics and Nanometer Structures Processing, Measurement, and Phenomena* **19**, 2508-2511, doi:10.1116/1.1421548 (2001).

101 Egerton, R. *Electron energy-loss spectroscopy in the electron microscope*. (Springer Science & Business Media, 2011).

102 Egerton, R. F. Radiation damage to organic and inorganic specimens in the TEM. *Micron* **119**, 72-87, doi:https://doi.org/10.1016/j.micron.2019.01.005 (2019).

103 Krasheninnikov, A. V. & Nordlund, K. Ion and electron irradiation-induced effects in nanostructured materials. *J. Appl. Phys.* **107**, 071301, doi:10.1063/1.3318261 (2010).

104 Susi, T. *et al.* Towards atomically precise manipulation of 2D nanostructures in the electron microscope. *2D Materials* **4**, 042004 (2017).

105 Susi, T. *et al.* Atomistic Description of Electron Beam Damage in Nitrogen-Doped Graphene and Single-Walled Carbon Nanotubes. *ACS Nano* **6**, 8837-8846, doi:10.1021/nn303944f (2012).

106 Banhart, F., Kotakoski, J. & Krasheninnikov, A. V. Structural Defects in Graphene. *ACS Nano* **5**, 26-41, doi:10.1021/nn102598m (2011).

107 Komsa, H.-P. *et al.* Two-Dimensional Transition Metal Dichalcogenides under Electron Irradiation: Defect Production and Doping. *Phys. Rev. Lett.* **109**, 035503, doi:10.1103/PhysRevLett.109.035503 (2012).

108 Meyer, J. C. *et al.* Accurate Measurement of Electron Beam Induced Displacement Cross Sections for Single-Layer Graphene. *Phys. Rev. Lett.* **108**, 196102 (2012).

109 Egerton, R. F. Control of radiation damage in the TEM. *Ultramicroscopy* **127**, 100-108, doi:https://doi.org/10.1016/j.ultramic.2012.07.006 (2013).

110 Shu, Y., Fales, B. S. & Levine, B. G. Defect-Induced Conical Intersections Promote Nonradiative Recombination. *Nano Lett.* **15**, 6247-6253, doi:10.1021/acs.nanolett.5b02848 (2015).

111 Bandara, H. M. D. & Burdette, S. C. Photoisomerization in different classes of azobenzene. *Chem. Soc. Rev.* **41**, 1809-1825, doi:10.1039/C1CS15179G (2012).

112 Waldeck, D. H. Photoisomerization dynamics of stilbenes. *Chem. Rev.* **91**, 415-436, doi:10.1021/cr00003a007 (1991).

113 Turro, N. J., Ramamurthy, V., Ramamurthy, V. & Scaiano, J. C. *Principles of molecular photochemistry: an introduction*. (University science books, 2009).

114 David, L., Panchapakesan, G., Jacek, J. & Bobby, S. *First Principles Determination of Electronic Excitations Induced by Charged Particles*. (2019).

115 Tsubonoya, K., Hu, C. & Watanabe, K. Time-dependent density-functional theory simulation of electron wave-packet scattering with nanoflakes. *Phys. Rev. B* **90**, 035416, doi:10.1103/PhysRevB.90.035416 (2014).

116 Ueda, Y., Suzuki, Y. & Watanabe, K. Quantum dynamics of secondary electron emission from nanographene. *Phys. Rev. B* **94**, 035403, doi:10.1103/PhysRevB.94.035403 (2016).

117 Tapavicza, E., Bellchambers, G. D., Vincent, J. C. & Furche, F. Ab initio non-adiabatic molecular dynamics. *PCCP* **15**, 18336-18348 (2013).

118 Schleife, A., Kanai, Y. & Correa, A. A. Accurate atomistic first-principles calculations of electronic stopping. *Phys. Rev. B* **91**, 014306, doi:10.1103/PhysRevB.91.014306 (2015).

119 Dutta, A. & Sherrill, C. D. Full configuration interaction potential energy curves for breaking bonds to hydrogen: An assessment of single-reference correlation methods. *The Journal of Chemical Physics* **118**, 1610-1619, doi:10.1063/1.1531658 (2003).

120 Cohen, A. J., Mori-Sánchez, P. & Yang, W. Insights into Current Limitations of Density Functional Theory. *Science* **321**, 792-794, doi:10.1126/science.1158722 (2008).

121 Ross, F. M. Opportunities and challenges in liquid cell electron microscopy. *Science* **350**, doi:10.1126/science.aaa9886 (2015).

122 Schneider, N. M. *et al.* Electron–Water Interactions and Implications for Liquid Cell Electron Microscopy. *The Journal of Physical Chemistry C* **118**, 22373-22382, doi:10.1021/jp507400n (2014).
123 LeCun, Y., Bengio, Y. & Hinton, G. Deep learning. *Nature* **521**, 436, doi:10.1038/nature14539 (2015).
124 Litjens, G. *et al.* Deep learning as a tool for increased accuracy and efficiency of histopathological diagnosis. *Scientific Reports* **6**, 26286, doi:10.1038/srep26286

https://www.nature.com/articles/srep26286#supplementary-information (2016).
125 Jean, N. *et al.* Combining satellite imagery and machine learning to predict poverty. *Science* **353**, 790 (2016).
126 Ziatdinov, M., Maksov, A. & Kalinin, S. V. Learning surface molecular structures via machine vision. *npj Computational Materials* **3**, 31, doi:10.1038/s41524-017-0038-7 (2017).
127 Ziatdinov, M. *et al.* Deep Learning of Atomically Resolved Scanning Transmission Electron Microscopy Images: Chemical Identification and Tracking Local Transformations. *ACS Nano* **11**, 12742-12752, doi:10.1021/acsnano.7b07504 (2017).
128 Maksov, A. *et al.* Deep learning analysis of defect and phase evolution during electron beam-induced transformations in WS2. *npj Computational Materials* **5**, 12, doi:10.1038/s41524-019-0152-9 (2019).
129 Madsen, J. *et al.* A Deep Learning Approach to Identify Local Structures in Atomic-Resolution Transmission Electron Microscopy Images. *Advanced Theory and Simulations* **0**, 1800037, doi:10.1002/adts.201800037 (2018).
130 Vasudevan, R. K. *et al.* Mapping mesoscopic phase evolution during E-beam induced transformations via deep learning of atomically resolved images. *npj Computational Materials* **4**, 30, doi:10.1038/s41524-018-0086-7 (2018).
131 Kirkland, E. J. *Advanced computing in electron microscopy*. (Springer Science & Business Media, 2010).
132 Badrinarayanan, V., Kendall, A. & Cipolla, R. SegNet: A Deep Convolutional Encoder-Decoder Architecture for Image Segmentation. *IEEE Transactions on Pattern Analysis and Machine Intelligence* **39**, 2481-2495, doi:10.1109/TPAMI.2016.2644615 (2017).